Naval Research Laboratory
Washington, DC 20375-5320

U.S. NAVAL RESEARCH LABORATORY

NRL/6810/MR—2023/3

Antimonide Photonic Power Converters Assembled Through Micro-Transfer Printing

MARGARET A. STEVENS

Quantum and Optoelectronics Branch
Electronics Sciences and Technology Division

September 21, 2023

DISTRIBUTION STATEMENT A: Approved for public release; distribution is unlimited.

REPORT DOCUMENTATION PAGE

Form Approved
OMB No. 0704-0188

Public reporting burden for this collection of information is estimated to average 1 hour per response, including the time for reviewing instructions, searching existing data sources, gathering and maintaining the data needed, and completing and reviewing this collection of information. Send comments regarding this burden estimate or any other aspect of this collection of information, including suggestions for reducing this burden to Department of Defense, Washington Headquarters Services, Directorate for Information Operations and Reports (0704-0188), 1215 Jefferson Davis Highway, Suite 1204, Arlington, VA 22202-4302. Respondents should be aware that notwithstanding any other provision of law, no person shall be subject to any penalty for failing to comply with a collection of information if it does not display a currently valid OMB control number. **PLEASE DO NOT RETURN YOUR FORM TO THE ABOVE ADDRESS.**

1. REPORT DATE *(DD-MM-YYYY)*	**2. REPORT TYPE**	**3. DATES COVERED** *(From - To)*
21-09-2023	NRL Memorandum Report	8/29/2022 – 8/28/2023

4. TITLE AND SUBTITLE

Antimonide Photonic Power Converters Assembled Through Micro-Transfer Printing

5a. CONTRACT NUMBER

5b. GRANT NUMBER

5c. PROGRAM ELEMENT NUMBER
NISE

6. AUTHOR(S)

Margaret A. Stevens

5d. PROJECT NUMBER

5e. TASK NUMBER

5f. WORK UNIT NUMBER
N21N

7. PERFORMING ORGANIZATION NAME(S) AND ADDRESS(ES)

Naval Research Laboratory
4555 Overlook Avenue, SW
Washington, DC 20375-5320

8. PERFORMING ORGANIZATION REPORT NUMBER

NRL/6810/MR--2023/3

9. SPONSORING / MONITORING AGENCY NAME(S) AND ADDRESS(ES)

Naval Research Laboratory
4555 Overlook Avenue, SW
Washington, DC 20375-5320

10. SPONSOR / MONITOR'S ACRONYM(S)

NRL-NISE

11. SPONSOR / MONITOR'S REPORT NUMBER(S)

12. DISTRIBUTION / AVAILABILITY STATEMENT

DISTRIBUTION STATEMENT A: Approved for public release; distribution is unlimited.

13. SUPPLEMENTARY NOTES

Karles Fellowship

14. ABSTRACT

This memorandum presents research conducted by Dr. Margaret Stevens (Code 6812) during her Jerome and Isabella Karle Distinguished Scholar Fellowship from August 29, 2022 – August 28, 2023. It details the design of a GaSb-based photonic power converter (PPC) which generates electrical power from eye-safe radiation as well as utilization of microscale transfer printing to optimize device performance under high optical power densities.

15. SUBJECT TERMS

16. SECURITY CLASSIFICATION OF:			**17. LIMITATION OF ABSTRACT**	**18. NUMBER OF PAGES**	**19a. NAME OF RESPONSIBLE PERSON**
a. REPORT	**b. ABSTRACT**	**c. THIS PAGE**			Margaret A. Stevens
U	U	U	U	15	**19b. TELEPHONE NUMBER** *(include area code)* (202) 404-4548

Standard Form 298 (Rev. 8-98)
Prescribed by ANSI Std. Z39.18

This page intentionally left blank.

CONTENTS

1. INTRODUCTION 1

2. APPROACH 2
   2.1 Design and fabrication of (Al)GaSb PPCs 2
   2.2 Micro-transfer printing of GaSb materials 3

3. EXPERIMENTS 5
   3.1 (Al)GaSb device performance 5
   3.2 GaSb membrane release and transfer printing 6
      3.2.1 HF-based etch chemistry 6
      3.2.2 Citric acid based etch chemistry 7
      3.2.3 AlGaAsSb membranes and transfer printing. 8

4. CONCLUSIONS 9

This page intentionally left blank.

EXECUTIVE SUMMARY

This report presents research conducted by Dr. Margaret Stevens (Code 6812) during her Jerome and Isabella Karle Distinguished Scholar Fellowship from August 29, 2022 – August 28, 2023. It details the design of a GaSb-based photonic power converter (PPC) which generates electrical power from eye-safe radiation. Devices were simulated in NRL MULTIBANDS® and optimized to maximize power conversion efficiency under 1550 nm monochromatic light. The highest efficiency was predicted for a device alloyed with a small amount of aluminum, $Al_{0.03}GaSb$, which increased the bandgap and maximized the voltage of the device. Simulated devices were grown by molecular beam epitaxy and processed in NRL's Nanoscience Institute. Although predicted performance of devices with AlGaSb was higher than GaSb, actual performance suffered due to low minority carrier lifetimes. This indicates that epitaxial material quality of low Al-containing antimonides needs optimization. In parallel to device optimization, the process for micro-transfer printing of antimonides was investigated using previously developed selective etch chemistries. Antimonide membranes were released from their native substrates and printed onto silicon handles. Increasing the temperature of the selective etch bath was found to decrease the time to release 200 x 200 μm membranes without adversely impacting etch selectivity.

This page intentionally left blank.

ANTIMONIDE PHOTONIC POWER CONVERTERS ASSEMBLED THROUGH MICRO-TRANSFER PRINTING

1. INTRODUCTION

Laser power beaming (LPB) enables long range, wireless power transfer from point of generation to point of need. This method power delivery can be agile and resilient – eliminating the need for bulky batteries or risky refueling convoys. Utilizing monochromatic light from a laser source, optical power is transmitted through the atmosphere and absorbed by a photovoltaic device at the receiving end. The specialized photovoltaic device, otherwise known as a photonic power converter (PPC), can be designed to efficiently convert the monochromatic radiation into electricity, with state of the art devices achieving 74.7% power conversion efficiency [1].

However, efficiency is not the only concern when designing LPB systems. Safety of the system is of paramount importance when sending high densities of optical energy through free space. Figure 1 shows the power conversion efficiency as a function of incident laser wavelength for various PPC technologies. While the highest efficiencies to date have been achieved around 808 nm using gallium arsenide (GaAs) PPCs, the maximum permissible exposure (MPE) for this laser wavelength is approximately 0.005 W/cm^2, or 1/20th the strength of the sun at Earth's surface [2]. To meet the energy demands of the battlespace, we will need to transmit and utilize significantly higher power densities. Although Figure 1 shows that the power conversion efficiency of existing PPCs decrease as a function of wavelength, the eye safety increases with wavelength, enabling much higher MPEs and the ability to transmit more power. For example, at 1550 nm the MPE would be 1 W/cm^2, a 500X improvement over that at 808 nm. As shown in Figure 1, the power conversion efficiency of devices at 1550 nm need optimization but theoretically could achieve efficiencies nearing 69%.

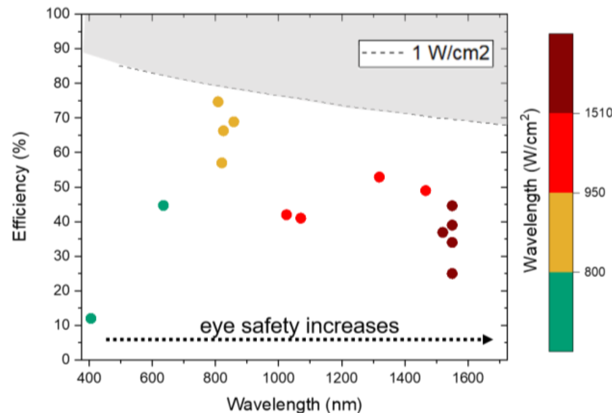

Fig. 1 — Efficiency of select photonic power converters as a function of the laser wavelength [1], [3], [12]–[15], [4]–[11]. As laser wavelength increases, eye safety increases. The theoretical maximum power conversion efficiency as a function of wavelength is also depicted by the dashed gray line.

Manuscript approved September 7, 2023.

Under very high optical power densities, the performance of large area photovoltaics can suffer due to resistive heating, metal grid-shadowing, and thermal effects. Microcell devices can offer improved performance under high optical power densities. Less than 1 mm^2 in area, microcells can offer some advantages over their large area counterparts including passive heat dissipation due to large perimeter-to-area ratios. When combined with techniques such as microscale transfer printing (µTP), microcells can be combined heterogeneously with effective heat dissipating surfaces such as diamond or aluminum nitride. While micro-transfer printing techniques are well developed to support devices operating at 808 nm, there are material challenges that need to be overcome to enable micro-transfer printing of devices operating at 1550 nm.

This program sought to address both of the above components of LPB research: development of an eye-safe PPC as well as utilization of microscale transfer printing to optimize device performance under high optical power densities. Gallium antimonide (GaSb) based devices were designed in NRL MULTIBANDS® and grown by molecular beam epitaxy (MBE). Devices were electrically characterized and tested with a low-power 1550 nm laser. Simultaneously, selective etch recipes were developed for removal of epitaxially grown GaSb membranes from the native substrate to enable heterogeneous integration by µTP. The efforts of this program resulted in a conference presentation and a journal manuscript in preparation. Additionally, the µTP development of GaSb compounds can be imminently leveraged in an ongoing 6.1 program investigating GaSb-based light emitters for neurophotonics applications.

2. APPROACH

2.1 Design and fabrication of (Al)GaSb PPCs

Devices were simulated in NRL MULTIBANDS® using the analytical model and a monochromatic 1550 nm input source at a power density of 0.1 W/cm^2. The (Al)GaSb device characteristics are shown in Figure 2 (a) and (b). The layer thicknesses, doping, and composition were optimized by maximizing power conversion efficiency. Both devices used the same window layer comprising of $Al_{0.1}GaSb$ of 10 nm and n-type doping of 2×10^{18} cm^{-2}, and back surface field (BSF) layer comprising of $Al_{0.1}GaSb$ at 25 nm and p-type doping of 1×10^{18} cm^{-2}. Figure 2(c) shows light current-voltage (LIV) simulations of a GaSb-based PPC compared to an $Al_{0.03}GaSb$ PPC. Including a small amount of Al in the active layer of the device results in a small decrease in short-circuit current density (J_{SC}), but a larger increase in open-circuit voltage (V_{OC}) and ultimately increases the power conversion efficiency by 7% relative. Further increasing the Al-fraction does not further increase the power conversion efficiency as the band gap is no longer optimal for the 1550 nm incident spectrum.

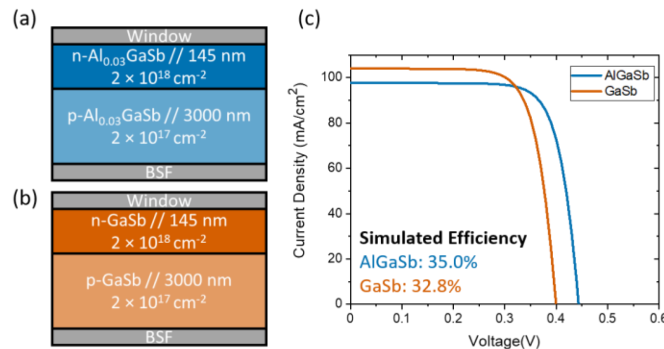

Fig. 2 — Device schematics of the (a) AlGaSb and (b) GaSb photonic power converters simulated in this work. (c) Simulated LIV characteristics of both devices under 0.1 W/cm^2 of monochromatic 1550 nm light.

Simulated devices were grown by solid-source MBE on the Riber 21 Compact DZ system. In situ wafer temperature was monitored using a pyrometer calibrated to the (2×5) to (1×3) transition while heating GaSb under a Sb_2 overpressure equivalent to 1 ML/s (414 °C). The oxide was removed from epi-ready (100) GaSb substrate by ramping to 545-550 °C under Sb flux. The sample was cooled to 490 °C and a 500 nm GaSb buffer was grown at 1 ML/s with a V/III flux ratio of 1.10. Subsequent device layers were grown under similar conditions to the buffer, with silicon used as the p-type dopant and gallium telluride (GaTe) used as the n-type dopant. The devices were capped with 10 nm of n-InAs doped with silicon to 1×10^{19} cm^{-2} to aid with making Ohmic contacts to the n-type material.

After growth, x-ray diffraction was used to measure the lattice constant and strain state, and the film composition was modeled to fit the data. Differential interference contrast microscopy (Nomarski) was used to evaluate the as-grown surface quality, monitoring for roughness or defects resulting from mixed group-V growth. Devices were processed in NRL's Nanoscience Institute using chemical etching, photolithography, and metal deposition and subsequently characterized in 6800's solar cell characterization facility. Electrical characterization included dark IV (DIV), external quantum efficiency (EQE), and testing under a 1550 nm laser source.

2.2 Micro-transfer printing of GaSb materials

In previous work by our group, we explored the etch selectivity of chemical etchants applied to various compounds lattice-matched to GaSb. To enable successful epitaxial lift-off (ELO) and micro-transfer printing of devices, near-infinite etch selectivity is desired. However, in the antimonide family, etch selectivity ratios are typically on the order of ~100. This creates difficulties during device separation, as the etching solution will etch the device appreciably alongside the sacrificial layer. Previously, our group has characterized etch selectivity between AlGaAsSb/InAsSb lattice matched to GaSb when using citric acid-based etches as well as hydrofluoric acid (HF) based etches [16]. Using 1:5 ratios of citric acid ($C_6H_8O_7$) and hydrogen peroxide (H_2O_2), an etch selectivity ratio of 852 was found between InAsSb/$Al_{0.33}$GaAsSb, with InAsSb etching at a rate of 554 nm/min. Alternatively, using an etch mixture of 1:1:100 HF:H_2O_2:H_2O cooled to 10 °C yielded an etch rate of >8000 nm/min for AlGaAsSb, but only resulted in an etch selectivity ratio of 171.5 for AlGaAsSb/InAsSb. The impact of cooling the etch solution temperature and varying the solution concentration was reported, and the surface was monitored for changes in roughness and oxidation. However, the results that were reported came from vertical etch tests where mesas were patterned into the surface to create step-edges to measure changes in etch depth along the (001) crystallographic direction. To selectively release a GaSb-based device, the etch plane will need to proceed laterally and undercut the mesa to be released. In this work, I applied these promising etch selectivity chemistries to monitor the release of 2 µm thick GaSb membranes from their native substrates.

Table 1 — Etch selectivity of compounds lattice-matched to GaSb, as reported by Stevens et al. [16]

	$InAs_{0.91}$Sb (nm/min)	**$Al_{0.34}$Ga(As)Sb (nm/min)**	**Selectivity**
1:5 Citric:H_2O_2 25 °C	554	0.65	852.3
1:1:100 HF:H_2O_2:H_2O 10 °C	48	8230	171

GaSb membrane etch structures were grown by solid source molecular beam epitaxy (MBE) on a Riber 21 Compact DZ. In situ wafer temperature was monitored using a pyrometer calibrated to the (2×5) to (1×3) transition while heating GaSb under a Sb_2 overpressure equivalent to 1 ML/s (414 °C). The oxide was removed from epi-ready (100) GaSb substrate by ramping to 545-550 °C under Sb flux. The sample was cooled to 490 °C and a 500 nm GaSb buffer was grown at 1 ML/s with a V/III flux ratio of 1.10. After, an etch stop/sacrificial release layer/etch stop stack was grown, with each layer 500 nm thick. $InAs_{0.91}Sb_{0.09}$ (hereafter known as InAsSb) layers were grown at 490 °C using an In growth rate of 1 ML/s, and a V/III flux ratio of 1.407, with the ratio of As to Sb tuned to achieve lattice matching to GaSb. $Al_{0.36}Ga_{0.64}As_{0.03}Sb_{0.97}$ (hereafter known as AlGaAsSb) layers were grown at 490 °C using a total group III growth rate of 1 ML/s and a V/III flux ratio of 1.10. For compatibility with the citric acid-based etchant, InAsSb was used as the sacrificial release layer and AlGaAsSb was used as the etch-stop layer. For the HF-based etchant, the AlGaAsSb was the sacrificial release layer, and the InAsSb the etch-stop layer. Finally, 2 µm of GaSb or AlGaAsSb was grown on top of the stop/release/stop stack with the same conditions as used for the buffer layer. After growth, x-ray diffraction was used to measure the lattice constant and strain state, and the film composition was modeled to fit the data. Differential interference contrast microscopy (Nomarski) was used to evaluate the as-grown surface quality, monitoring for roughness or defects resulting from mixed group-V growth.

For membrane release experiments, the GaSb membranes and the first etch-stop layer were patterned into mesas with side lengths of 200 µm. The membranes were coated with 45 nm of SiN_x and 90 nm of SiO_2 deposited by plasma-enhanced chemical vapor deposition (PECVD), for additional sidewall protection. The mask used for the dielectric bilayer includes openings for metal contacts for future devices; however, there is no metal deposited on the GaSb membranes. Then, trenches were etched through the sacrificial layer and the bottom etch stop layer. Finally, photoresist was patterned to further protect the GaSb membrane and tether it to the underlying etch stop layer. The entire process flow and Nomarski microscopy images of 200 x 200 µm mesas at each step is shown in Figure 3.

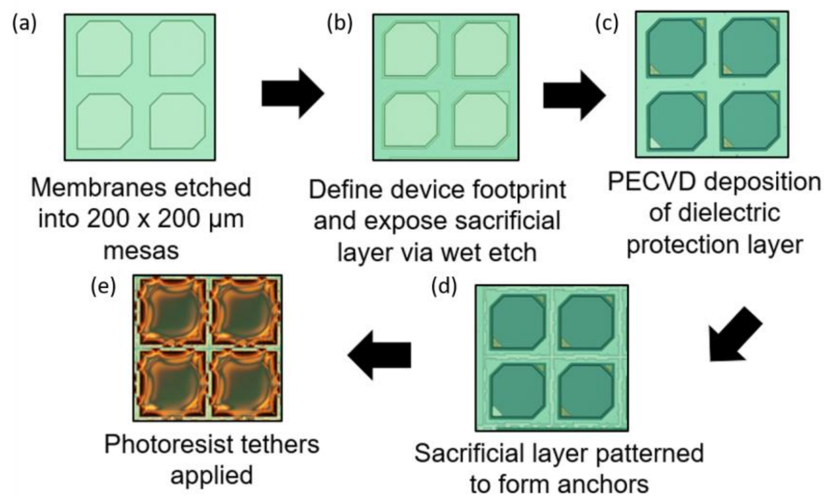

Fig. 3 — Nomarski images of the process flow for micro-transfer printing of GaSb and AlGaAsSb membranes including (a) mesa definition, (b) device footprint definition, (c) plasma-enhanced chemical vapor deposition of the dielectric protection layer, (d) chemical etch into sacrificial layer to form anchor points, and (e) photoresist tethers applied.

Chemicals used for selective etching included combinations of 49% hydrofluoric acid (HF), citric acid comprising of equal parts $C_6H_8O_7$ mixed with deionized water, and 30% hydrogen peroxide (H_2O_2). Etch solutions were mixed in a beaker surrounded by a water bath inside of an ultrasonic cleaning unit with temperature control. The temperature of the water bath was monitored with a thermometer and agreed with the temperature of the etch solution within ±5°C. To achieve the desired etch temperatures, the water

bath was either heated using the temperature controls on the ultrasonic unit, or cooled with the addition of ice to the bath. The etch solution was mixed and placed in the water bath for 1 hour prior to etching for the temperature to stabilize. The samples were immersed in the etch solution in 30–90 min intervals. After each etch time interval, samples were rinsed with DI water, dried with N2, and imaged with a Nomarski microscope and an infrared (IR) microscope. For select samples, the photoresist tethers were removed with a bath of acetone and isopropanol and the samples were tilted to 52° and imaged with scanning electron microscopy (SEM) using a Helios microscope.

3. EXPERIMENTS

3.1 (Al)GaSb device performance

Figure 4 shows a suite of electrical characterization for the fabricated GaSb (orange) and AlGaSb (blue) devices. From the DIV in Figure 4(a), we can see that both devices look similarly. Unfortunately, there is high dark current in reverse bias, ~100 mA/cm^2, indicating issues with leakage pathways in both devices. NRL MULTIBANDS® numerical simulations (not shown) indicate dark current should be on the order of 0.1 mA/cm^2; therefore, there are non-idealities that are occurring in these devices that need to be mitigated. One solution could be optimizing the doping in the base of the devices. While the doping level of 2×10^{17} cm^{-2} was chosen to optimize the power conversion efficiency in the analytical model, that high level of doping may be detrimental in practice to the dark current and resulting performance of the device. Another solution could be material optimization. There was a high density of surface defects, on the order of 1×10^{3} cm^{-2}, of unknown origin on these samples. We are investigating whether these are "spitting defects" which originate from one of our sources and cause metal-rich localized defects.

Figure 4(b) shows the EQE for the GaSb and AlGaSb devices. While the DIV look very similar between the two devices, the EQE looks very different. The peak EQE for GaSb is 52%, while for AlGaSb it was 29%. This indicates serious issues with material quality in the AlGaSb layer which ultimate impact the ability of the device to convert incident photons into electrical current. Other authors have seen poor EQE in AlGaSb solar cells [17] and attributed this to poor carrier transport and reduced minority carrier lifetimes. Optimization of the AlGaSb material quality could be improved through lattice-matching by incorporating As into the crystal and by manipulating growth conditions including temperature and V/III flux ratios. The latter may prove to be the most important, as the peak EQE of the GaSb device was 52% while simulations show it should have been 59%, which indicates our antimonide growth conditions need improvement in general.

Finally Figure 4(c) shows the performance of the GaSb PPC under a 1550 nm laser. The laser power density is approximated to be 0.018 W/cm^2 using the EQE profile to approximate the expected short-circuit current under the 0.1 W/cm^2 incident spectrum. Ultimately, the power conversion efficiency of the device is quite low due to the shunting effects seen in the DIV. The LIV curve is linear, rather than diode-like, resulting in a very low FF and V_{OC}. Future work includes developing new GaSb and AlGaSb PPCs with lower doping in the base and optimized antimonide growth conditions.

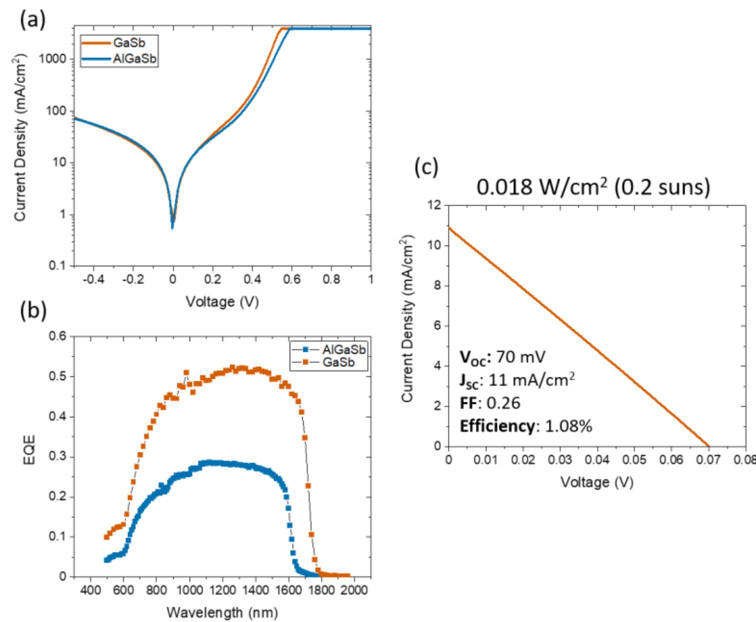

Fig. 4 — Electrical characterization of GaSb (orange) and AlGaSb (blue) devices including (a) DIV (b) EQE and (c) LIV under 0.018 W/cm^2 monochromatic 1550 nm light.

3.2 GaSb membrane release and transfer printing

To evaluate the different etch chemistries explored in previous work [16], three different samples were investigated (1) HF-based etch sample which used AlGaAsSb as the sacrificial layer and InAsSb as the etch-stop layers, (2) citric acid-based etch sample which used InAsSb as the sacrificial layer and AlGaAsSb as the etch-stop layers, and (3) an alternative version of the citric-based etch sample that used AlGaAsSb as the membrane to be released. This enabled the use of an IR microscope to monitor the progression of the lateral etch.

3.2.1 HF-based etch chemistry

While the HF-based etch chemistry did not have the highest etch selectivity, it was able to provide a very fast etch rate of the sacrificial layer. If the lateral etch rate is the same as the vertical etch rate of AlGaAsSb, a 200 µm cell could be undercut in as little as 13 minutes. Figure 4(a) shows a cross-sectional schematic of the HF-based etch chemistry sample. GaSb membranes approximately 2 µm thick were grown on top of a stack of InAsSb/AlGaAsSb/InAsSb each with layer thicknesses of 500 nm. The etched mesas were capped with a SiN_x/SiO_2 coating and a top layer of protective photoresist. The sample was immersed in a solution of 1:1:100 $HF:H_2O_2:H_2O$ at 10 °C to maximize etch selectivity between the InAsSb and AlGaAsSb. Figure 4(b) shows Nomarski microscope images of the sample before etching as well as after 90 minutes of immersion in the solution. The after image is stripped of the photoresist protective layer. From the top-view microscope image, it appears as though the surrounding AlGaAsSb layer has been etched away and only remains underneath where the resist was present (top right and bottom left corners). However, the membranes were still adhered to the native substrate. IR microscopy images (not shown) did not provide any indication whether the samples had been undercut by the etch after 90 minutes.

To monitor how the etch was progressing laterally, a small section of each sample was cleaved off and imaged with SEM at a tilt angle of 52°. Images of the HF-based sample are shown in Figure 5(c).

While indeed most of the sacrificial layer around the microcell was etched away, and some undercutting of the mesas did occur during the 90 minutes, the bottom etch-stop layer was completely consumed and the etch proceeded into the GaSb substrate. Our previous work showed InAsSb, the etch-stop layer in this case, was etched at rate of 48 nm/min in this etch chemistry. Therefore, it is likely the 500 nm etch stop layer disappeared after approximately 10 minutes of exposure to the etch solution. While further time immersed in the HF-based etchant may lead to fully undercut membranes, the membranes will no longer be tethered to that underlying etch stop layer, and it would be difficult to print using transfer-printing techniques. Future optimization of this etch could include eliminating the H_2O_2 from the etch solution chemistry to slow down the InAsSb etch rate. However, the lateral etch rate of AlGaAsSb still may not be fast enough to undercut the samples before the InAsSb underlayer is consumed.

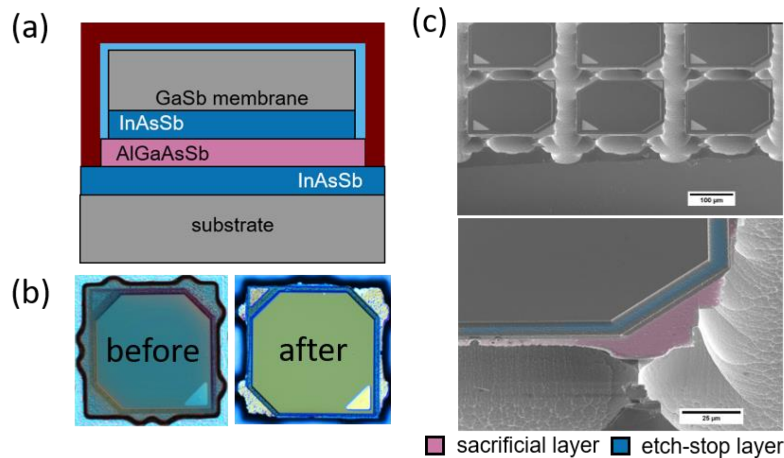

Fig. 5 — (a) Cross-sectional schematic of the HF-based etch sample. (b) Top-down view of Nomarski microscopy images of the etch test sample before and after immersion in the etch solution for 90 minutes. (c) Tilted SEM images of membranes after etching in solution for 90 minutes.

3.2.2 Citric acid based etch chemistry

From previous work, we had found that the citric acid-based etch chemistry yielded the highest etch selectivity between AlGaAsSb and InAsSb, but had a much slower etch rate of sacrificial layer when compared to the HF-based etch. Figure 6(a) shows a cross-sectional schematic of the citric acid based etch, with AlGaAsSb as the etch-stop layer and InAsSb as the sacrificial layer. The sample was immersed in 1:4 citric acid:H_2O_2 for 90-minute intervals. Figure 6(b) shows Nomarski images (top) and IR microscopy images (bottom) of the sample after 0, 180, and 360 minutes. After 180 minutes, a white “ring” appears around the membrane where the top-etch stop layer is present. The AlGaAsSb etch stop layer has a bandgap of 1.16 eV and therefore is transparent to the near-IR microscope light. The bright contrast visible to the IR microscope is likely from an air pocket that forms underneath the AlGaAsSb layer that has been undercut. After 360 minutes, the sacrificial layer has retreated further under the GaSb membrane. Because GaSb’s bandgap is 0.73 eV, it is not transparent to the near-IR microscope and therefore the microscope cannot further monitor the undercutting of the membrane.

Figure 6(c) shows tilted-SEM images of the sample exposed to the citric acid-based etch for 180 minutes. In contrast to the sample exposed to the HF etch, the bottom etch-stop layer still remains around the mesas. The InAsSb sacrificial layer (light pink) appears to be etching laterally at a much slower rate than the vertical 554 nm/min measured previously. However, it is receding underneath the membrane, creating the desired undercutting effect. Nomarski imaging of the areas around the sample did not show

color change that would be indicative of oxidation of the Al-containing layers. Therefore, AlGaAsSb is found to be very stable in the citric-acid based etch, and is well suited as an etch-stop layer.

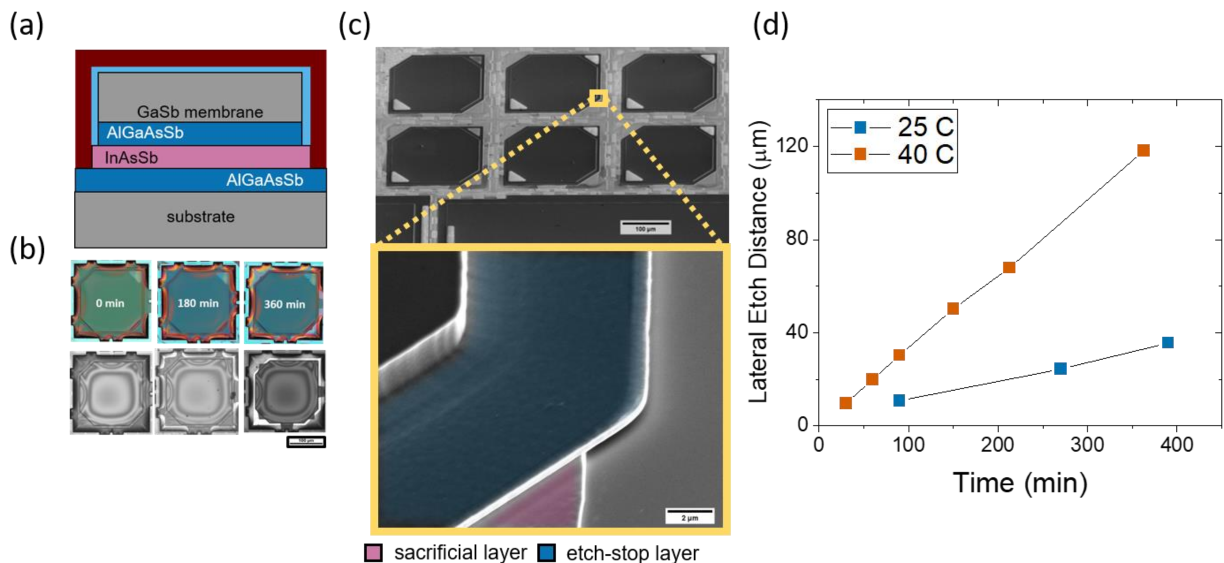

Fig. 6 — (a) Cross-sectional schematic of citric-acid based etch test sample. (b) Nomarski (top) and IR microscopy (bottom) images after 0, 180, and 360 min in the etch solution bath at 25 °C. (c) Tilted cross-sectional SEM images of the sample etched for 180 minutes at 25 °C. (d) Lateral etch distance as a function of time for etch solutions at 25 °C (blue squares) and 40 °C (orange squares).

To quantify the difference between the vertical etch rate previously measured, and the lateral etch rates seen here, a combination of IR microscopy and peel tests were used to monitor the receding of the InAsSb sacrificial layer. Figure 6(d) shows the lateral etch distance as a function of time when the solution was at 25 °C (blue squares). The slope of the line gives an etch rate of 92 nm/min, less than 20% of the vertical etch rate. This shows that vertical etch rates are not the best predictor of undercut rates for transfer printable membranes. If this etch rate stays stable, the time to undercut the membranes would be 21 hours but the bottom etch-stop layer would be completely consumed in this time frame. In previous work, we had looked at reducing the temperature of the etching solution as a way to increase etch selectivity, but found that the InAsSb and AlGaAsSb etch rates decreased by similar amounts, rendering a similar etch selectivity. However, we did not explore the impact of elevated temperature on the etch rates and subsequent etch selectivity. Figure 6(d) shows the lateral etch distances as a function of time for the InAsSb when in a solution of 40 °C, yielding a lateral etch rate of ~330 nm/min. This would fully etch the membranes in approximately 6 hours.

3.2.3 AlGaAsSb membranes and transfer printing.

To further study the lateral etch rate of InAsSb in citric acid-based solutions, I grew a new sample shown by the cross-sectional schematic in Figure 7(a). This sample used 2 µm of AlGaAsSb as the membrane to allow for IR microscopy to monitor the full process of undercutting the mesa. The InAsSb sacrificial layer was thickened to 1000 nm and the bottom etch-stop layer was thickened to 1000 nm as well. Figure 7(b) shows the lateral etch distance as a function of time for the sample placed in 1:4 citric:H_2O_2 at 40 °C. The lateral etch progresses steadily at a rate of 310 nm/min until full release. This is encouraging, as it indicates the etch is not slowing down with time due to membrane bending or other view-factor issues. Figure 7(c) shows Nomarski images of the etch as it progresses, from starting morphology to fully released. Over time, the dark region, corresponding to the InAsSb sacrificial layer,

recedes in a square-shape until it fully disappears and a ring-like interference pattern remains. This pattern indicates the membrane is fully undercut and is ready for transfer-printing.

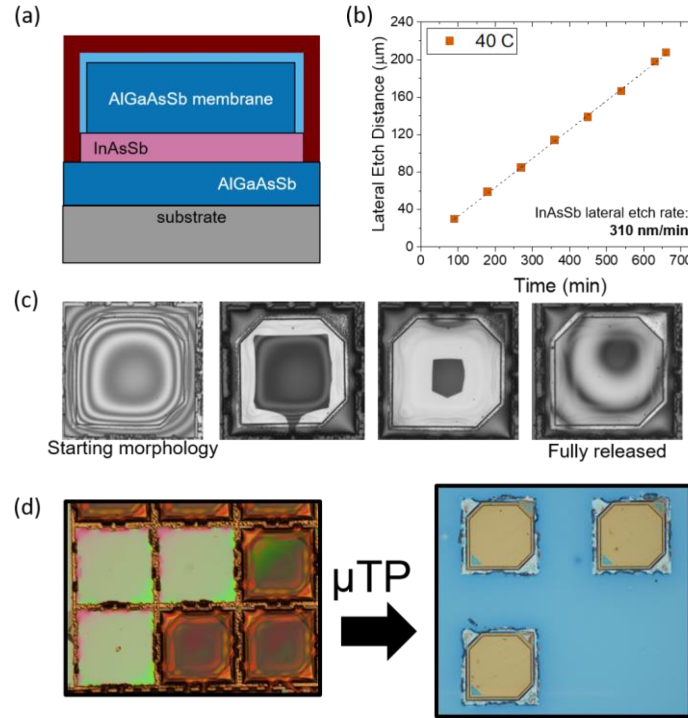

Fig. 7 — (a) Cross-sectional schematic of the AlGaAsSb membrane sample. (b) Lateral etch distance as a function of time for the sample in 1:4 citric:H_2O_2 at 40 °C. (c) IR Microscopy images of the sample, from staring morphology through fully released. (d) Sample after µTP, showing the empty spaces left on the native substrate (left) and the membranes transferred to a silicon handle (right).

Figure 7(d) shows AlGaAsSb membranes before and after transfer printing onto a silicon handle wafer. Three membranes were fully released (left) and transfer printed onto silicon coated with a thin print adhesive (right). After transfer printing the top layer of photoresist was stripped with a solvent bath. All three chiplets were still tethered to the underlying substrate, enabling easy pick-and-place transfer of the membranes. To improve the yield of the release process, the sample would need to be returned to the etch solution for longer to ensure more chiplets have been fully undercut by the InAsSb etch process.

4. CONCLUSIONS

Overall, this program sought to develop an eye-safe PPC as well as utilize microscale transfer printing to optimize device performance under high optical power densities. (Al)GaSb devices were simulated in NRL MULTIBANDS® and grown by molecular beam epitaxy (MBE). Including a small amount of Al in the active layer of the device results in a small decrease in short-circuit current density (J_{SC}), but a larger increase in open-circuit voltage (V_{OC}) and ultimately increases the power conversion efficiency by 7% relative. Devices were electrically characterized and tested with a low-power 1550 nm laser. While simulations predicted higher power conversion efficiencies, fabricated devices were plagued with shunting defects that resulted in degraded performance. Future work includes developing new GaSb and AlGaSb PPCs with lower doping in the base and optimized antimonide growth conditions. Simultaneously, selective etch recipes were developed for removal of epitaxially grown GaSb membranes from the native substrate to enable heterogeneous integration by µTP. Using a 1:4 ratio of citric acid and H_2O_2 at 40 °C resulted in the full release of AlGaAsSb membranes in 7 hours and subsequent transfer

printing onto a silicon handle. Future work involves applying this selective etch technique to release GaSb-based photovoltaics and LEDs to test their electrical performance before and after the etch-release process.

REFERENCES

[1] S. Fafard and D. P. Masson, “74.7% Efficient GaAs-Based Laser Power Converters at 808 nm at 150 K,” *Photonics*, vol. 9, no. 8, p. 579, Aug. 2022, doi: 10.3390/photonics9080579.

[2] Laser Institute of America, “American National Standard for Safe Use of Lasers,” Orlando, FL, 2007. [Online]. Available: https://webstore.ansi.org/standards/lia/ansiz1362007.

[3] M. A. Green, J. Zhao, A. Wang, and S. R. Wenham, “45% Efficient Silicon Photovoltaic Cell Under Monochromatic Light,” *IEEE Electron Device Lett.*, vol. 13, no. 6, pp. 317–318, 1992, doi: 10.1109/55.145070.

[4] S. J. Wojtczuk, “Long-wavelength laser power converters for optical fibers,” *Conf. Rec. IEEE Photovolt. Spec. Conf.*, pp. 971–974, 1997, doi: 10.1109/pvsc.1997.654250.

[5] J. Mukherjee, S. Jarvis, M. Perren, and S. J. Sweeney, “Efficiency limits of laser power converters for optical power transfer applications,” *J. Phys. D. Appl. Phys.*, vol. 46, no. 26, 2013, doi: 10.1088/0022-3727/46/26/264006.

[6] V. P. Khvostikov *et al.*, “GaSb laser-power (λ = 1550 nm) converters: Fabrication method and characteristics,” *Semiconductors*, vol. 50, no. 10, pp. 1338–1343, 2016, doi: 10.1134/S1063782616100146.

[7] S. Fafard *et al.*, “High-photovoltage GaAs vertical epitaxial monolithic heterostructures with 20 thin p/n junctions and a conversion efficiency of 60%,” *Appl. Phys. Lett.*, vol. 109, no. 13, 2016, doi: 10.1063/1.4964120.

[8] N. Singh, C. Kin Fai Ho, Y. Nelvin Leong, K. E. K. Lee, and H. Wang, “InAlGaAs/InP-Based Laser Photovoltaic Converter at ∼ 1070 nm,” *IEEE Electron Device Lett.*, vol. 37, no. 9, pp. 1154–1157, 2016, doi: 10.1109/LED.2016.2591015.

[9] C. De Santi *et al.*, “GaN-based laser wireless power transfer system,” *Materials (Basel).*, vol. 11, no. 1, 2018, doi: 10.3390/ma11010153.

[10] M. Beattie, “Semiconductor Materials and Devices for High Efficiency Broadband and Monochromatic Photovoltaic Energy Conversion,” 2021.

[11] H. Helmers *et al.*, “68.9% Efficient GaAs-Based Photonic Power Conversion Enabled by Photon Recycling and Optical Resonance,” *Phys. status solidi – Rapid Res. Lett.*, vol. 15, no. 7, p. 2100113, Jul. 2021, doi: 10.1002/pssr.202100113.

[12] S. V. Sorokina, F. Y. Soldatenkov, N. S. Potapovich, M. Z. Shvarts, and V. P. Khvostikov, “Au- and Ag-containing contacts to GaSbphotovoltaic converters,” *IEEE Electron Device Lett.*, vol. 3106, no. c, pp. 1–1, 2022, doi: 10.1109/led.2022.3148432.

[13] S. Fafard and D. P. Masson, “High-Efficiency and High-Power Multijunction InGaAs/InP

Photovoltaic Laser Power Converters for 1470 nm," *Photonics*, vol. 9, no. 7, p. 438, 2022, doi: 10.3390/photonics9070438.

[14] N. Javed, N.-L. Nguyen, S. F. Ali Naqvi, and J. Ha, "Long-range wireless optical power transfer system using an EDFA," *Opt. Express*, vol. 30, no. 19, p. 33767, Sep. 2022, doi: 10.1364/OE.468766.

[15] Y. Tai and T. Miyamoto, "Experimental Characterization of High Tolerance to Beam Irradiation Conditions of Light Beam Power Receiving Module for Optical Wireless Power Transmission Equipped with a Fly-Eye Lens System," *Energies*, vol. 15, no. 19, p. 7388, Oct. 2022, doi: 10.3390/en15197388.

[16] M. A. Stevens, J. A. Nolde, S. Mack, and K. J. Schmieder, "Selective Etching of 6.1 Å Materials for Transfer-Printed Devices," in *2022 IEEE 49th Photovoltaics Specialists Conference (PVSC)*, Jun. 2022, pp. 0240–0243, doi: 10.1109/PVSC48317.2022.9938631.

[17] E. Vadiee *et al.*, "AlGaSb-Based Solar Cells Grown on GaAs: Structural Investigation and Device Performance," *IEEE J. Photovoltaics*, vol. 7, no. 6, pp. 1795–1801, 2017, doi: 10.1109/JPHOTOV.2017.2756056.